bre

# Annex D – CFD modelling of Cavity Barrier Scenarios

## Introduction

BRE work on fire modelling research and development has culminated in the development of its own computational fluid dynamics (CFD) fire models JASMINE and SOFIE. In the current study, these models have been used to complement the experimental programmes, discussed in Annexes A and B, for assessing the performance of cavity barriers installed in:

- floor voids (Annex A), and
- plenum spaces (Annex B).

The experimental data from these scenarios have been used to further develop and validate simple fire growth and heat release rate sub-models, within JASMINE and SOFIE CFD models, so that the validated models can be used with confidence for investigating variations to both floor voids and plenum space designs.

## Mathematical Description of the CFD Modelling

The fluid dynamics and heat transfer associated with a fire are governed by the principles of conservation of mass, momentum, thermal energy and chemical species. These 'conservation laws' may each be expressed in terms of partial differential equations, the solution of which provides the basis for the CFD model. CFD models solve, numerically, the governing conservation equations in order to generate field values for velocity components, temperatures and concentrations of chemical species, such as the fire combustion products.

The solution of the governing flow equations requires the numerical discretisation of the flow domain into a finite number of cells or control-volumes. The discretisation of the flow domain must conform to boundaries in such a way that boundary conditions can be accurately represented. Furthermore regions with steep property gradients, such as at the fire source, must be discretised with a sufficiently fine grid.

The 'correct' design of the numerical grid and a sufficient grid resolution, as appropriate to a particular problem, are essential for obtaining realistic and reasonably accurate results from a CFD model.

JASMINE and SOFIE CFD models solve the three-dimensional transient RANS (Reynolds Averaged Navier Stokes) equations. BRE's large-scale experimental facilities have played an important role in underpinning the development and validation of these models. Validation of the CFD model is essential in ensuring trust and confidence in model predictions.

### Combustion modelling

In JASMINE and SOFIE, the fire is represented by means of a combustion model, by contrast to the simpler heat source models used in some simpler treatments of approaches. Two alternative treatments are available – the eddy-break-up model based in mixing control, which assumes fast chemistry, or the laminar flamelet model which incorporates more detailed chemistry via pre-computed scalar relationships thereby relaxing the fast chemistry assumption to some degree.

### Radiation modelling

Radiation is modelled by using the six-flux model or the discrete transfer radiation model coupled with wide-band emissive power model and a soot model. The discrete transfer model is more appropriate to prediction of flame spread where a more exact resolution of the radiative transfer is required than that afforded by the simpler “six-flux” radiation model.

### Turbulence modelling

The CFD model adopts the standard two-equation k-$\varepsilon$ turbulence model with buoyancy modification which has been used extensively for modelling turbulence in fires.

### Modelling flame spread

For the purposes of this study a “critical accumulated flux” flame spread model has been used. This model requires a number of material specific “constants” which range from physical parameters such as the material’s virgin and char densities to more general effective properties such as the heat of gasification. These types of models require calibration in the context of relatively simple combustion experiments, of which the cone calorimeter is a prime example. Whilst some guidance on the values of the parameters required can be extracted from literature or previous studies, a careful model calibration exercise is necessary for each material to ensure an accurate reproduction of the test conditions.

The procedure adopted for the calibration of the model constants is iterative and hard to define precisely. The main flame spread parameters which are adjusted are as follows:

- critical accumulated flux (directly affects time-to-ignition, but also spread rates)
- heat of gasification (affects rate of burning, once ignited)
- minimum heat flux (an effective loss term which reflects the fact that a certain critical flux is required to give ignition even at infinite times)
- volatile temperature (this is not an temperature threshold for ignition but is simply the temperature of volatiles released into the gas-phase from a pyrolysing surface; however, it is deemed unphysical for surface temperature to exceed this value during pyrolysis so this parameter does provide an effective cap on the re-radiation)

Other more minor flame spread model parameters define the time-dependence of the heat of gasification parameter and the densities of the virgin material and char layer. The material thickness is also specified so that burn-out, when the specimen is burnt right through, can be correctly represented in the model.

Other significant parameters not directly associated with flame spread are the assumed surface emissivity and the soot model constants, controlling sooting levels. The former parameter is particularly awkward because it is poorly known for some materials, it is expected to vary significantly with temperature, and it has a profound influence on the model representation of the surface heat transfer processes due to its appearance in the absorbed and emitted radiation terms.

The soot can be modelled by using a prescribed scalar approach. This simple engineered approach does not allow formation or destruction of soot but relies upon the fact that if an appropriate level is supplied at the boundary, then the correct concentration evolves in the main part of the first plume simply according to mixing. This may introduce some inaccuracies, as soot concentrations near the fire surface and more remotely from the fire plume may both be overpredicted. However, the model is robust and can be simply calibrated by using the ratios of peak yield data from small-scale tests.

**Table D1 Thermal properties of rock fibre used in the THELMA simulations[D1].**

| Temperature (ºC) | Conductivity (W/m/C) | Density (kg/m$^3$) | Specific heat (J/kg/C) |
|---|---|---|---|
| 10 | 0.0360 | 110 | 809 |
| 100 | 0.0469 | 110 | 876 |
| 200 | 0.0665 | 110 | 950 |
| 300 | 0.0880 | 110 | 1047 |
| 400 | 0.117 | 110 | 1150 |
| 600 | 0.190 | 110 | 1369 |
| 800 | 0.285 | 110 | 1635 |
| 900 | 0.340 | 110 | 1788 |

**Modelling temperature dependent material properties**

The thermal properties of the insulating materials such as Rock fibre can change significantly when exposed to high temperatures. BRE's thermal model THELMA [D2] is used to compute temperature parameters, for example, the thermal conductivity of the Rock fibre increases by a factor of 10 and its thermal capacity by a factor of two when it is exposed to increase in temperature from 10ºC to 900ºC, as shown in Table D1 below [D1]. It is therefore important to take into account the temperature dependence of thermal properties for accurate prediction of the insulation failure of the cavity barrier.

## Floor cavity barrier

The CFD model JASMINE was used to simulate the smoke and heat transfer characteristics for two of the floor void cavity fire tests discussed in Annex B, the Scenarios considered were:

Floor Test 3 : The floor cavity void was 300mm in height; the cavity barrier was located in the centre of the floor, and the fire source was 600 mm away from the cavity barrier, and was produced by a propane burner with heat release rate of 200kW.

Floor Test 4 : Floor Test 4 was identical to Floor Test 3 but with no cavity barrier in place.

The above data offers a means of assessing the effect of the presence of cavity barrier on thermal environment due to a fire inside the floor void space.

The floor slabs used in these tests were constructed from steel encapsulated chipboard panels. For the purposes of these simulations, the thermal properties of this floor panels were assumed to be that of the chipboard. The cavity barrier used was constructed from rock fibre. The thermal properties of these materials used in the CFD and THELMA simulation are given in Tables D1 and D2.

**Table D2 Thermal properties of Chipboard.**

| Material | Conductivity (W/m/C) | Density (kg/m$^3$) | Specific heat (J/kg/C) |
|---|---|---|---|
| Chipboard | 0.11 | 715 | 1590 |

### Floor Test 3

Figure D1 shows the geometrical configuration of the fire test scenarios. Since the fire was located centrally and symmetrically inside the floor cavity, by exploiting the symmetry, only half of the floor cavity void was needed for the CFD simulation.

Figures D2 and D3 show the movement of combustion products in terms of velocity vectors coloured with local gas temperatures inside the floor cavity void at the horizontal planes at 100 mm and 200 mm respectively above the ground. Figures D4 and D5 show the temperature contours in the horizontal planes at 100 mm and 200 mm respectively above the ground.

Figures D2 to D5 clearly show that the cold air (13$^o$C) is entrained into the fire at lower level and hot combustion products move away from the fire at higher level. This is in qualitative agreement with the observations in the tests.

Figure D6 shows the evolution of predicted temperature profile at the exposed surface of the cavity barrier facing the fire at 20mm, 80mm and 150mm from the suspended ceiling of the floor void. This surface temperature distribution was then used in BRE's thermal model THELMA to compute the temperature profile on the unexposed surface of the

cavity barrier. The temperature dependent thermal properties of the cavity barrier made of rock fibre, as shown in Table D1, were taken into account in the THELMA model.

Figure D7 shows the evolution of the predicted temperatures at the centre (25mm) and on the unexposed face of the cavity opposite the fire source. The predicted temperatures on mid cavity point (25mm) are also compared with the measurements and can be seen to be in reasonably good agreement. The predicted results show that the maximum temperature at the unexposed surface of the cavity barrier does not exceed the insulation failure criterion (average value of 140°C or maximum value of 180°C above ambient after 15 minutes) given by *Approved Document B,* which is in agreement with the measured test data. This suggests that the cavity barrier was effective in this case.

**Floor Test 4**

Figure D8 shows the scenario of Test 4 simulation.

Figure D9 and D10 show the velocity vectors on the horizontal planes at 100 mm and 200 mm respectively above the ground, and figure D11 shows the temperature contours on the horizontal plane at 200 mm above the ground. The predicted results clearly show that the cold air is entrained into the fire at lower level and hot smoke moves away from the fire at the higher level.

Figure D12 shows the temperature profile at the location where the unexposed surface of the cavity barrier is in Floor Test 3. The results show that the maximum temperature at this section (unexposed surface of the cavity barrier) is about 500$^{o}$C. This is in agreement with the test data that shows the temperature at the same location varies from 350$^{o}$C to 510$^{o}$C.

Compared with the simulation results presented in D9 and D10, it is concluded that the floor cavity barrier is effective when the height of the floor cavity is 300 mm. The 150 mm floor cavity could be similarly investigated using the same approach.

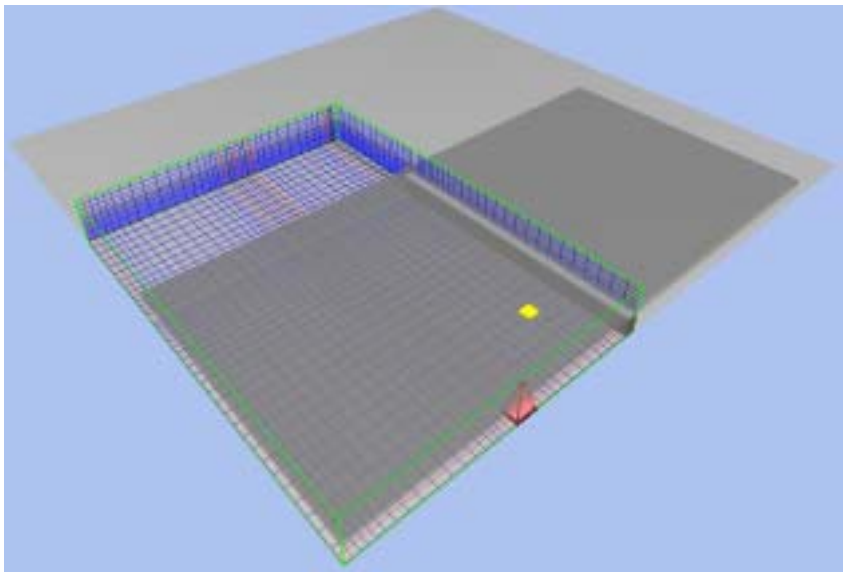

**Figure D1 Schematic representation of floor test 3 (with cavity barrier)**

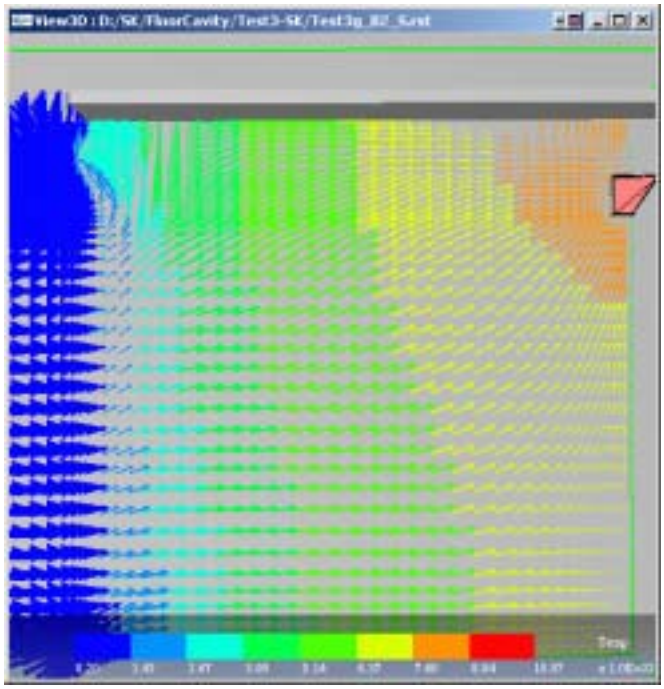

**Figure D2 Air movement at the horizontal plan 100 mm above the ground (Floor Test 3)**

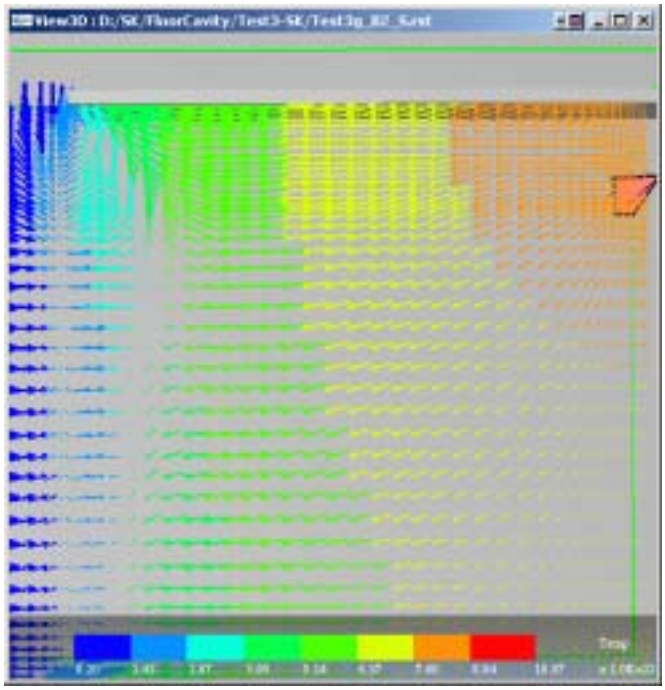

**Figure D3 Air movement at the horizontal plan 200 mm above the ground (Floor Test 3)**

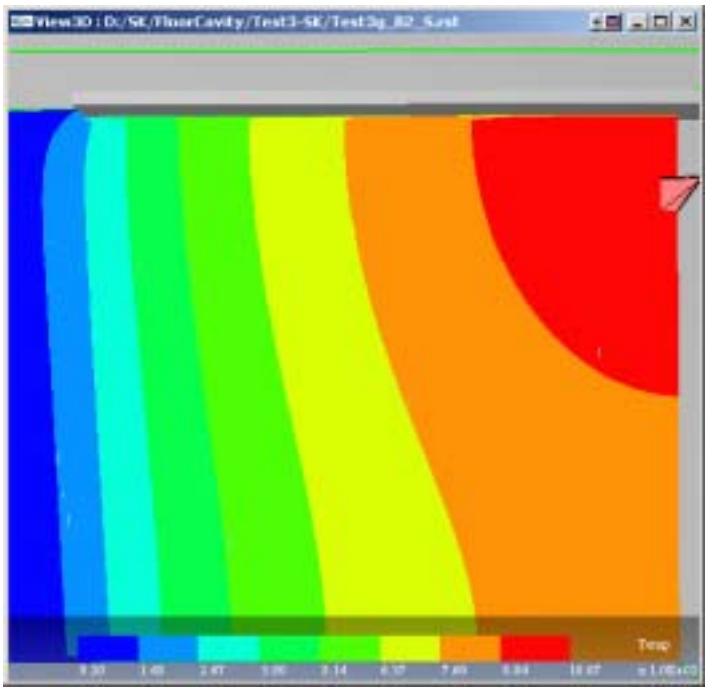

Figure D4 Temperature field at the horizontal plan 100 mm above the ground (Floor Test 3)

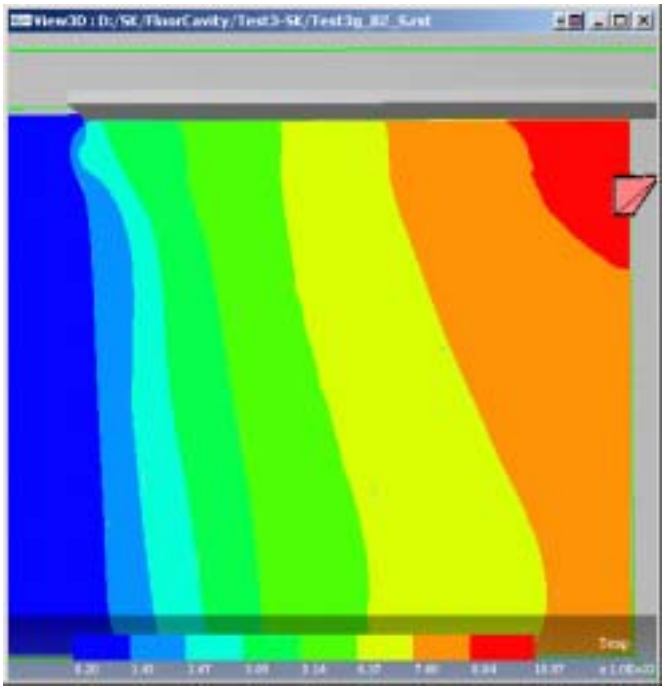

**Figure D5 Temperature field at the horizontal plan 200 mm above the ground (Floor Test 3)**

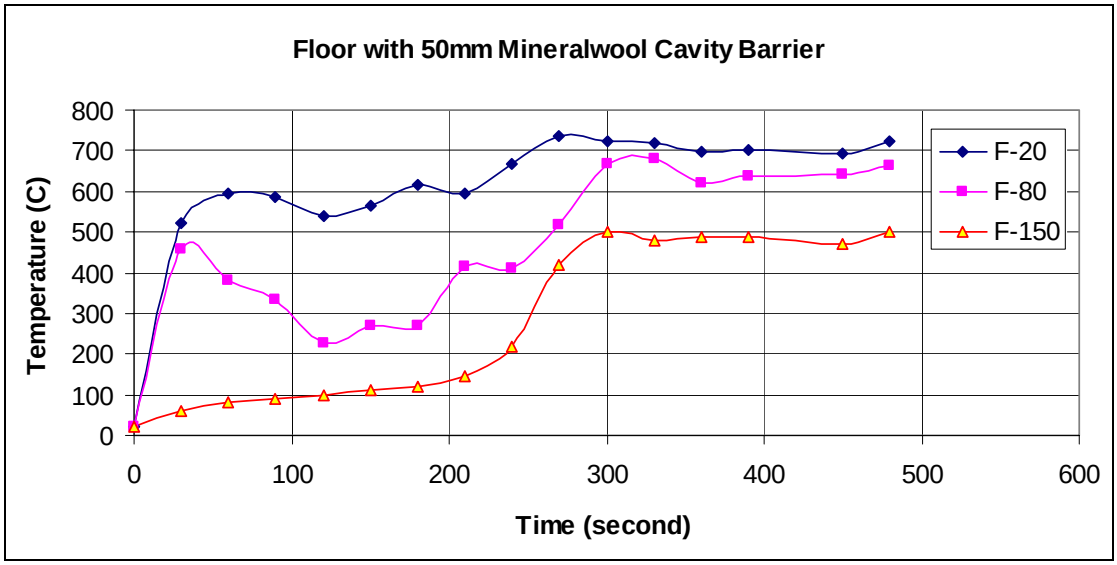


Figure D6 Evolution of predicted gas temperatures at the exposed surface of the cavity barrier ( Floor Test 3) (F-20 means 20 mm below the suspended ceiling of the floor void, etc)

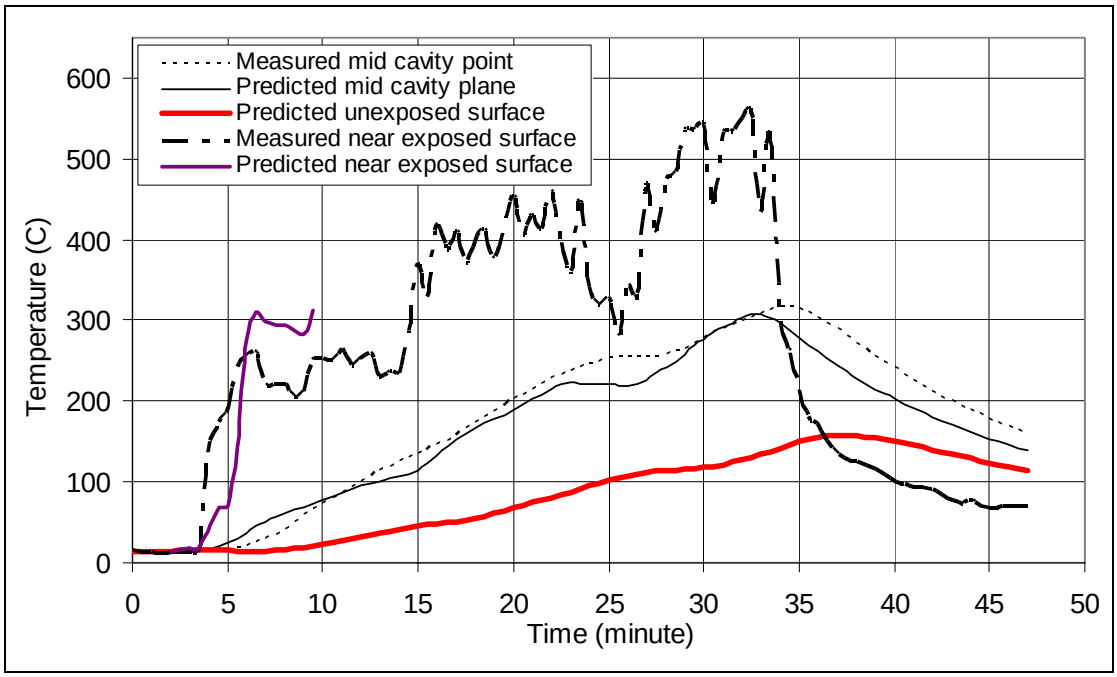


Figure D7 Temperature profile at the leeside surface of the cavity barrier that does not face the fire (Floor Test 3)

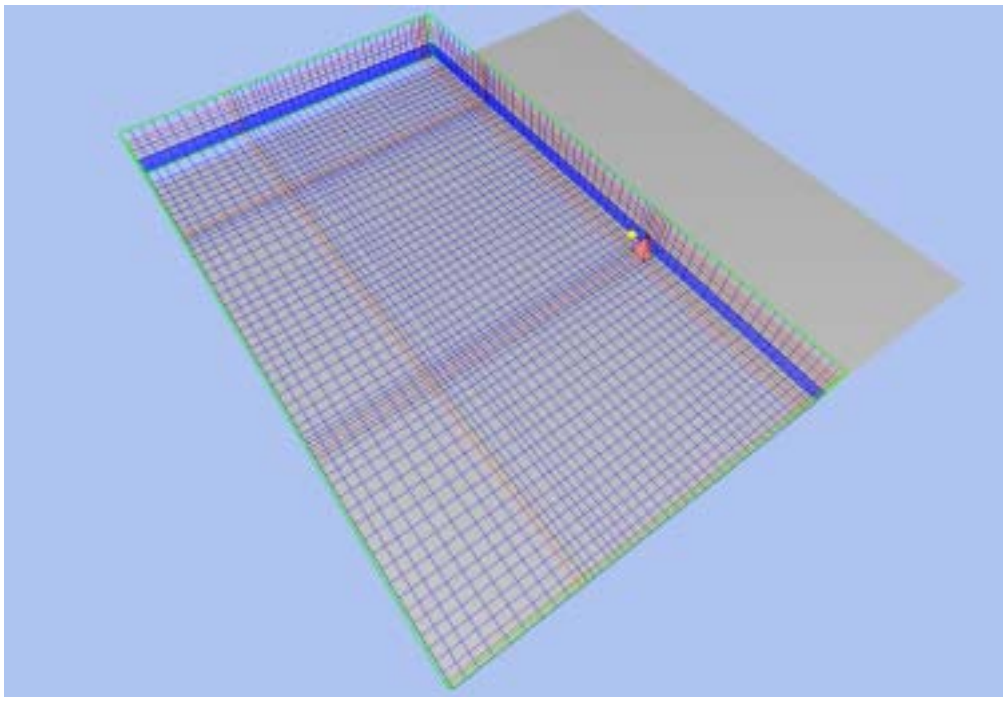

Figure D8 Schematic of Floor Test 4 with numerical grid

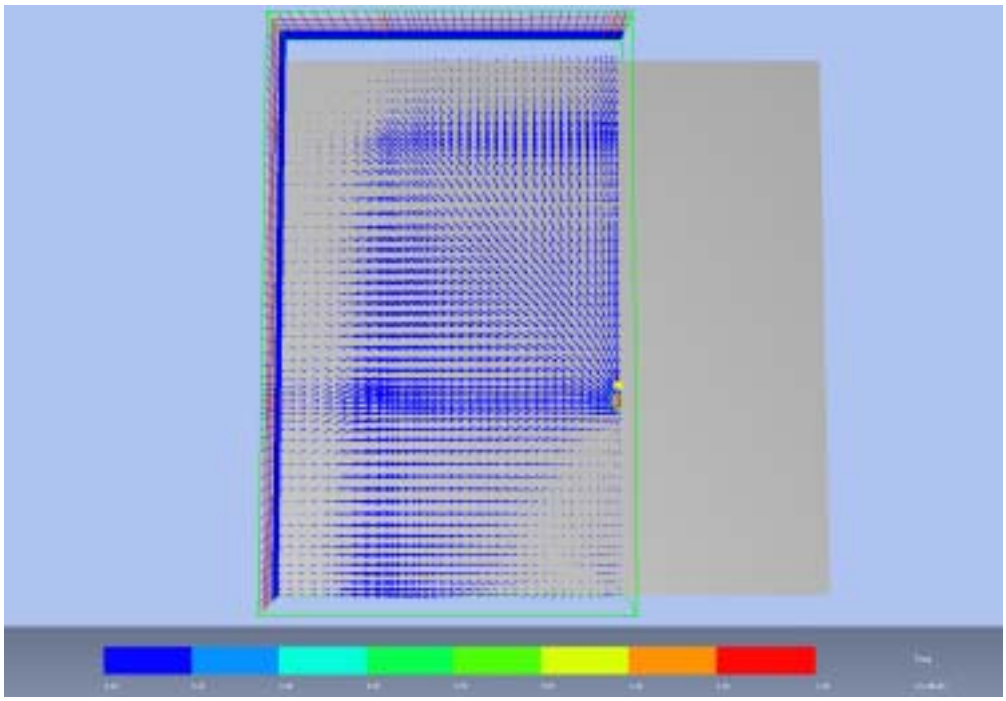

Figure D9 Air movement at the horizontal plan 100 mm above the ground (Floor Test 4)

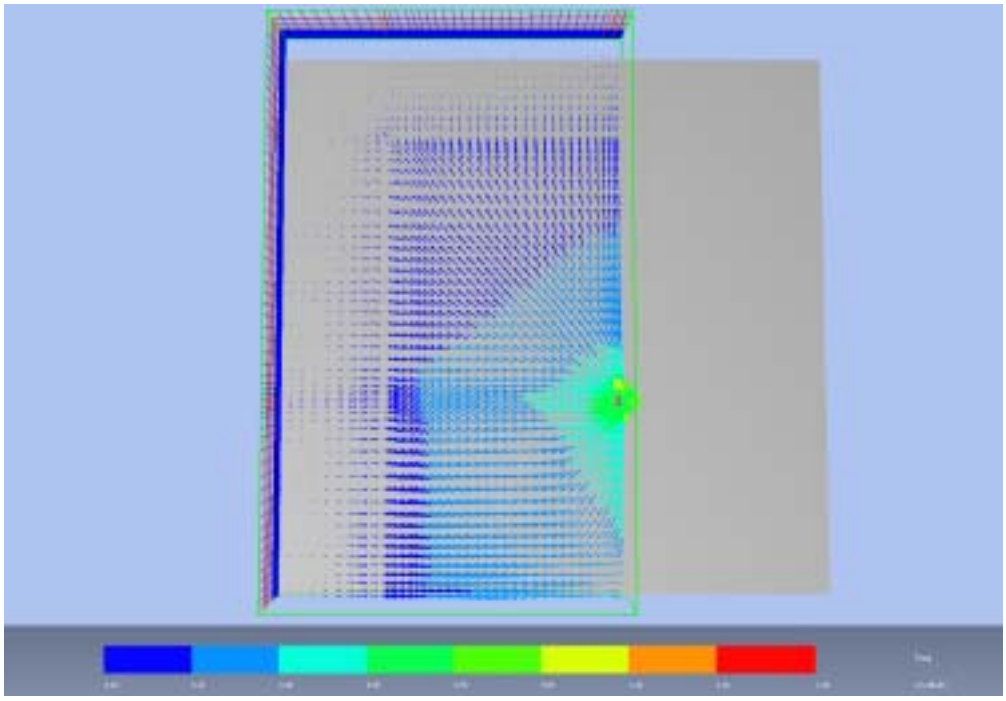

Figure D10 Air movement at the horizontal plan 200 mm above the ground (Floor Test 4)

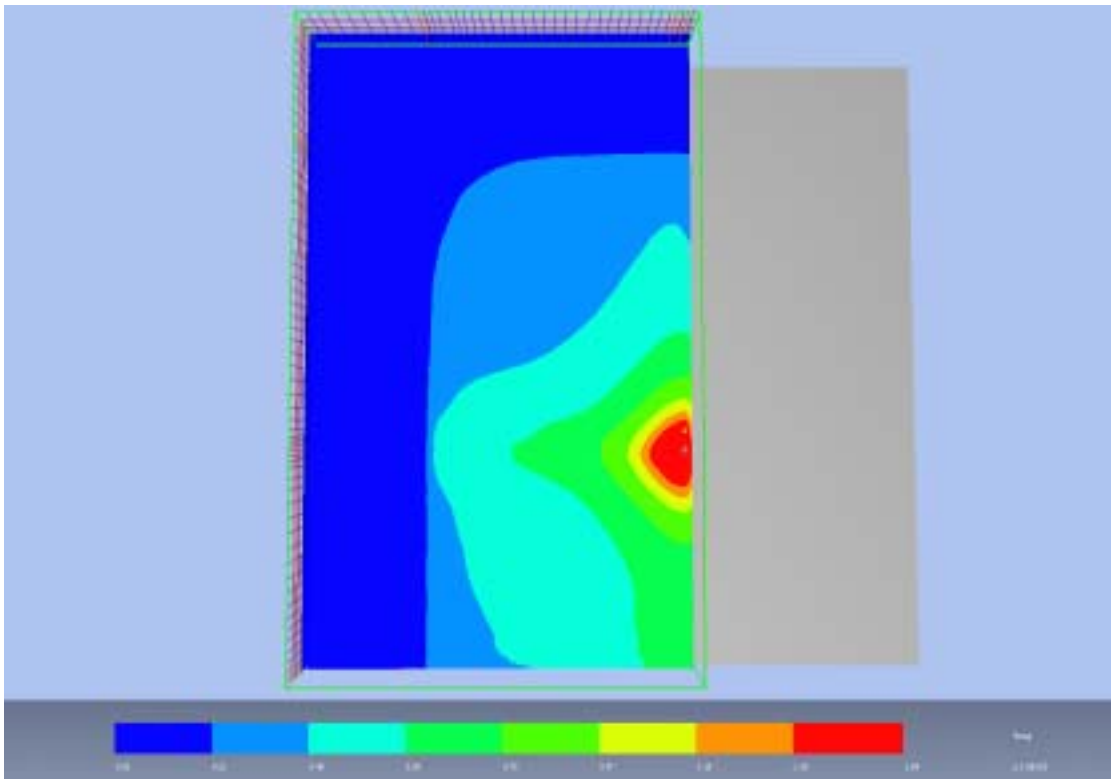

Figure D11 Gas temperature contours on the horizontal plane at 100 mm above the ground (Floor Test 4)

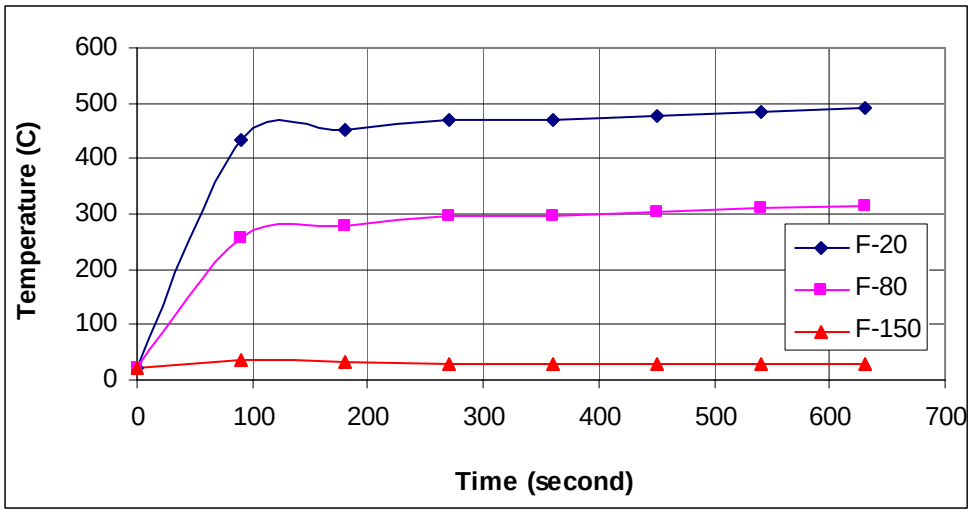


Figure D12 Evolution of the predicted gas temperatures at the position where the unexposed surface of the cavity barrier is in Floor Test 3 (Floor Test 4)

## Plenum space (ceiling void) scenario

### Experimental Details

Figure D13 shows a plan view of the plenum test rig. The rig was made of brick construction with internal dimensions of 7.37m in length, 5.76m in width and 4m in height. A suspended ceiling was installed at 3m from the floor to create a fire room below and a plenum space (ceiling void) above it. Full design details are presented in Annex A.

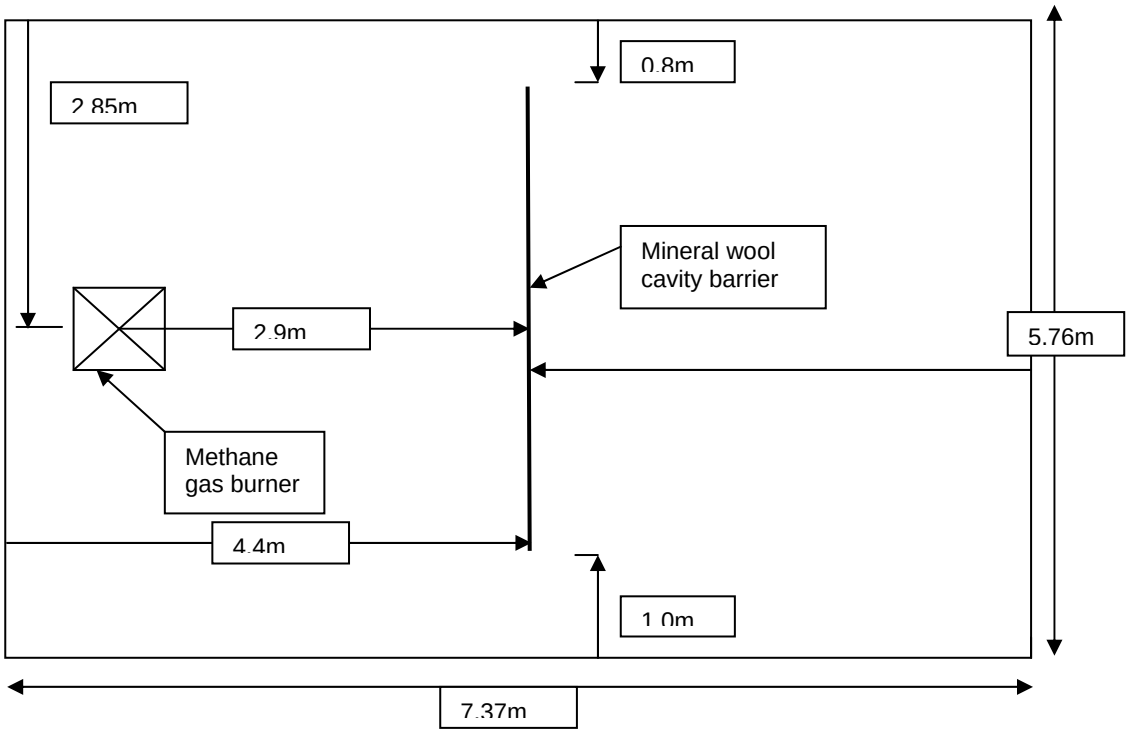


**Figure D13 Plan view of plenum test rig**

The gas burner was placed 2m below the suspended ceiling, with its centre being located 1.5m from the near burner end wall of the test rig. The suspended ceiling consisted of a suspended steel grid holding 0.6m x 0.6m x 9 mm thick calcium silicate ceiling tiles. The ceiling tile situated directly above the centre of the fire source had a 450 mm x 450 mm (0.2 $m^2$) hole cut in it to provide a breach into the ceiling void that provided ventilation in to the ceiling void. An additional tile in the centre of the back wall (burner end wall) was also removed to allow for additional ventilation in the ceiling (plenum) void. A high volume air extract system was fitted to the test rig, which extracted air from the ceiling void. The extract system had a controlled extract rate up to 11 $m^3/s$, exhausting into a 0.76m diameter horizontal duct through a 0.45 $m^2$ opening in the wall (extract end wall) remote from the gas burner. Please note that the ventilation for the replacement air was provided through the holes in the walls of the fire room, as shown in figure D14.

A ½ hr rated, rock fibre cavity barrier, was installed inside the ceiling void, 2.9m from the centre of breach hole, 4.4m from the fire end wall of the rig.

Three test scenarios were considered and are discussed in detail in Annex B.

## Details of computer modelling of the fire tests

Test 3 was used as the basis of the CFD modelling simulation.

### Modelling the Geometry, Cavity Barrier and Extraction System

Figure D15 shows the computer simulated schematic of the test rig with front end wall removed to view the fire room below and a ceiling void above the suspended ceiling. The figure shows the location of the extract system (green) in the end wall remote from the fire end and the cable bundle (pink) through the cavity barrier (grey) in the ceiling void (plenum space). The figure also shows a 1m square burner fire, with heat release rate of 1MW, which was located 1m above the floor and 2m below the suspended ceiling. The suspended ceiling included the breach hole, 0.45m by 0.45m in area, above the fire and another hole (0.6m by 0.8m in area) adjacent to the fire end wall to simulate a missing tile (0.6m by 0.6m) and some leakage in ceiling tiles above the burner fire and around the burning cable bundle.

Instead of modelling the individual holes in the walls, the lower half of the walls was modelled as open. The extraction system for test 3 was set at 2.16m$^3$/s, giving a flow velocity of some 4.8m/s.

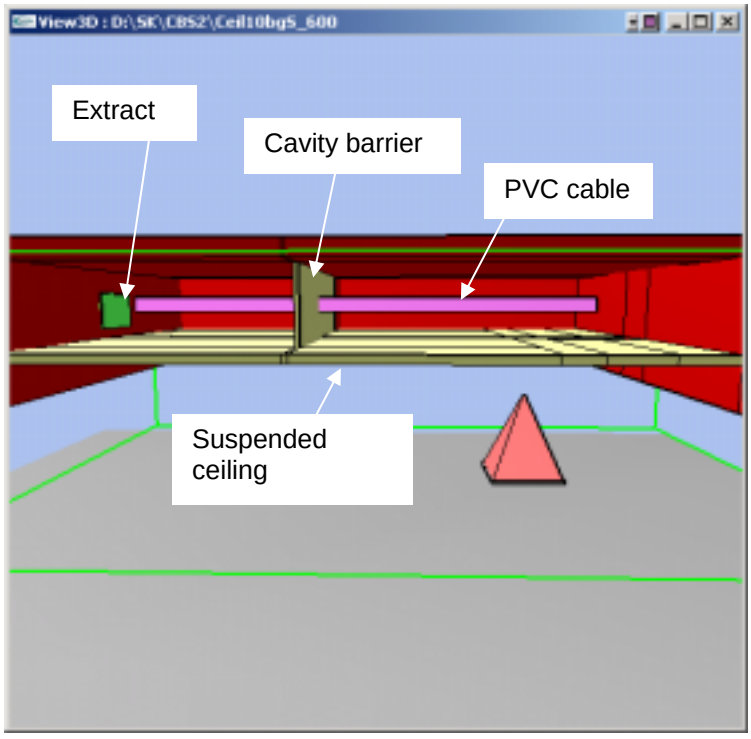


Figure D15 Computer simulated schematic of the test rig

**Thermal Properties of the materials**

To simulate heat transfer through the cavity barrier at elevated gas temperatures of around 500°C the following thermal properties were used:

- thermal conductivity 0.15 W/m/C,
- specific heat capacity 1250 J/kg/C and
- density was taken to be 110kg/$m^3$.

The thermal properties of the specific communication cable used in this study were not available and so the following properties were taken from previous work using similar cables:

- thermal conductivity 0.022W/m/C,
- specific heat 30900J/kg/C and
- density 2040kg/$m^3$ .

**Flame spread modelling of the PVC communication cable**

A cumulative flux model, described earlier, was used to model the flame spread on the PVC cable bundle. The minimum flux and critical accumulated flux for ignition of the cable were obtained by undertaking cone experiments on a 100mm by 100m sample (single sheet) of the PVC communication cable (5mm in diameter) at four incident flux levels, i.e., 50kW/$m^2$, 35kW/$m^2$, 25kW/$m^2$, and 15kW/$m^2$. By plotting the inverse square root of the time against the incident flux, as shown in Figure D16, the intersection of the extrapolated fitted line to the data at the incident flux axis gives the minimum flux for ignition, which comes to about 10kW/$m^2$ for the four-core unscreened PVC communication cable material used in this study. The cone tests gave time to ignition ($t_{ig}$) for the four incident fluxes ($q_{in}$)as follows:

$q_{in}$ = 50 kW/$m^2$, $t_{ig}$ = 10s

$q_{in}$ = 35 kW/$m^2$, $t_{ig}$ = 47s

$q_{in}$ = 25 kW/$m^2$, $t_{ig}$ = 111s

$q_{in}$ = 15 kW/$m^2$, $t_{ig}$ = 267s

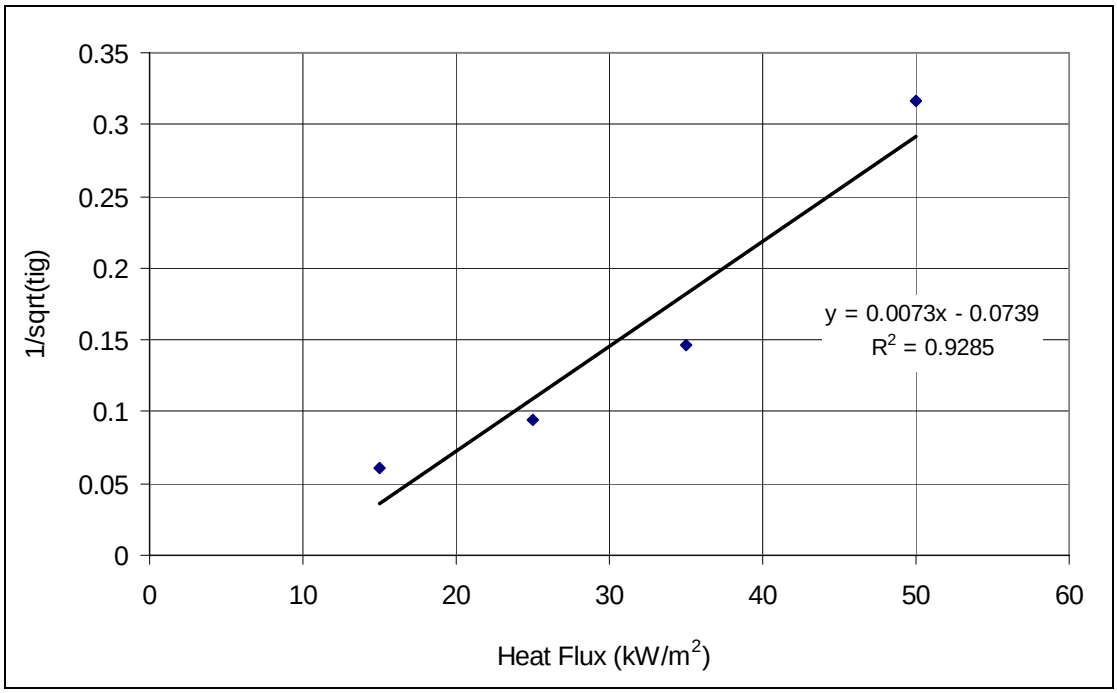


Figure D16 Determination of critical heat flux for ignition for the PVC communication cable using the cone data

The above cone data suggested significant variation in critical accumulated flux, ranging between 500MJ/m$^2$ and 3500MJ/m$^2$ for single layer of the PVC sample. In the full-scale ceiling test 3, the bundle of PVC cable involved several layers, and the flames from a 1MW burner provided the source of radiation for ignition of the cable, where the time to ignition of cable bundle was observed to be about 105s. Guided by the cone data, and taking into account the incident flux from 1MW burner flame on the cable surface, the critical accumulated flux was set to 2.0 MJ/m$^2$.

Since there was no data available for heat of gasification (Hg) of the PVC communication cable used in the test, a literature review suggested values ranging between 1 and 3 MJ/kg were typical. A parametric analysis was therefore undertaken to examine the sensitivity of the Hg value on the predicted results and it was found that it affected the distribution of heat released from the burning cable, the lower value giving a higher peak value. A value of 1.5MJ/kg for Hg corresponded well with measured peak value from the ceiling test 3. Other less critical parameters required by the critical accumulated flux model were chosen as follows:

Tv = 370°C, $\rho_{virgin}$= 2040kg/m$^3$, $\rho_{char}$= 25kg/m$^3$, $\delta_{mat}$ = 10mm, $Hg_1$= 0.8, $Hg_2$= 1,

where Tv is the volatilisation temperature of the PVC material, $\rho_{virgin}$ is the density of the material, $\rho_{char}$ is the density of the char left, and $Hg_1$ and $Hg_2$ are the two factors controlling the shape of the heat release rate curve from the PVC cable bundle.

**Numerical details**

The computational domain used for the numerical simulations is indicated in Figure D17 by the green lines. A total of approximately 60,000 numerical grid cells (52x39x30) were used for the extended computation of 10m by 7m in plan and 4.1m in height. A fixed pressure boundary was used on the extended computational boundaries to ensure correct flow through the open boundaries in the fire room.

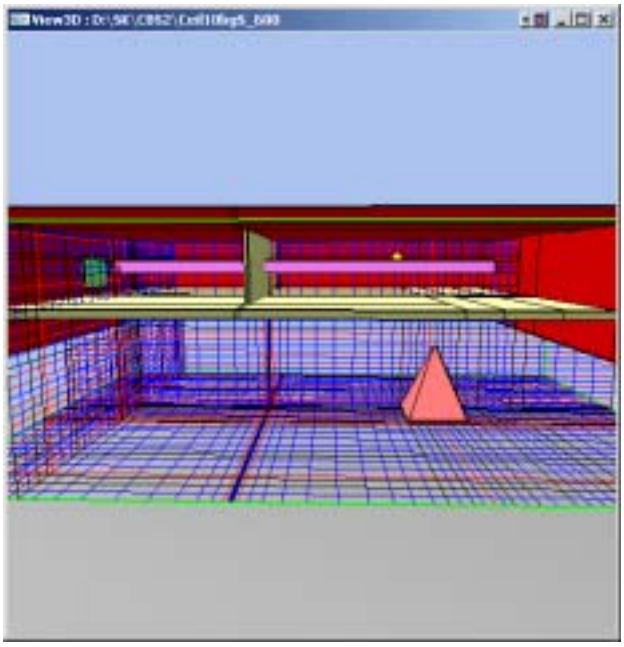

Figure D17 Schematic of the test rig with numerical grid (front wall removed)

**Results and discussion**

Figures D18 to D19 respectively show the predicted gas temperature contours in the plenum space on the vertical central plane through the fire and the cavity barrier, and on the horizontal central plane through the barrier and the burning cable. The yellow colour from the key at the bottom of the key suggests temperature ranging between 700°C and 800°C (or 1000 and 1110 K) surrounding the cavity barrier. The velocity vectors in Figure D20 illustrate the fact that the uniform temperature on the exposed and unexposed side of the cavity barrier is caused due to recirculation of hot combustion products from the burner flames and the burning PVC communication cable. The high temperatures on both the exposed and unexposed faces of the cavity barrier, shown in Figures D21 and D22 respectively, are caused due to this recirculation of combustion products in the plenum space. Figures D23 and D24 illustrate respectively the incident radiative flux on the PVC cable and extent of burning of its top surface. Figure D25 shows the heat release of the burning PVC communication cable as predicted by the model, which, in

view of the uncertainty in material property data, shows satisfactory agreement with the measured peak heat release rate of 426kW.

## References – Annex D


1. Guy, P. Private Communication.
2. Kirby, J.A. & Welch, S. (2000) "THELMA - A finite-element package for solving two-dimensional thermal problems - User Guide", BRE, 59 p.


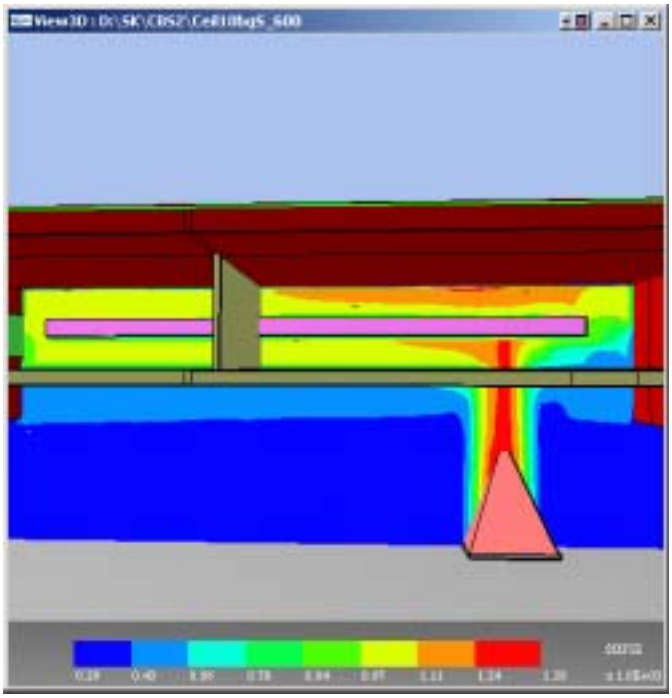

**Figure D18 Temperature contours on the vertical central plane through the fire and cavity barrier**

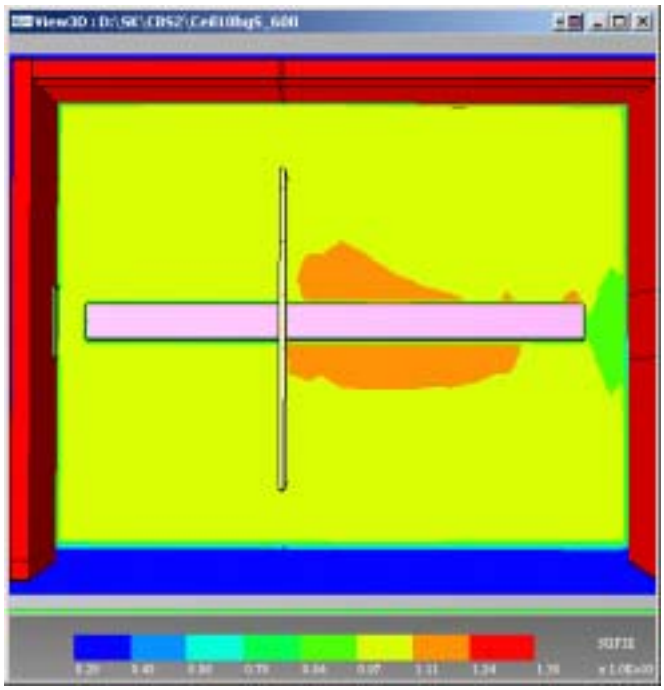

**Figure D19 Temperature contours at centre of plenum space on the horizontal central plane through the cavity barrier and the burning cable**

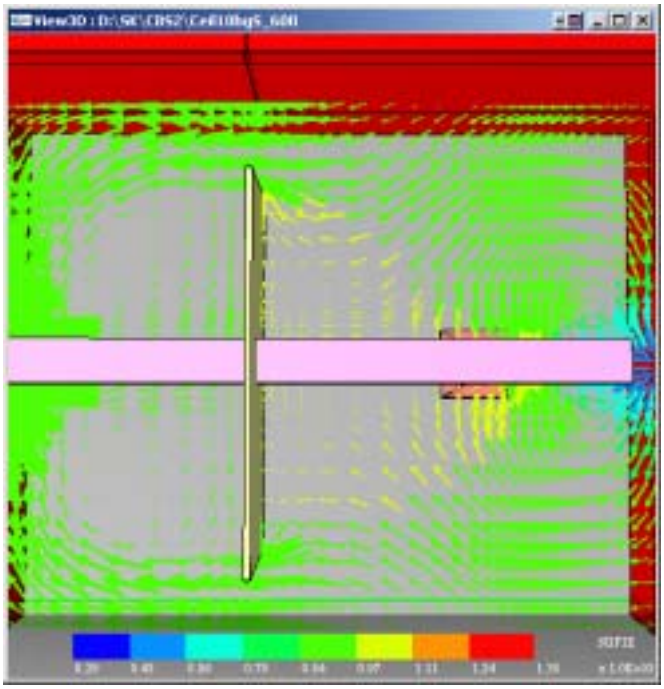

**Figure D20 Temperature contours at centre of plenum space on the horizontal central plane through the cavity barrier and the burning cable**

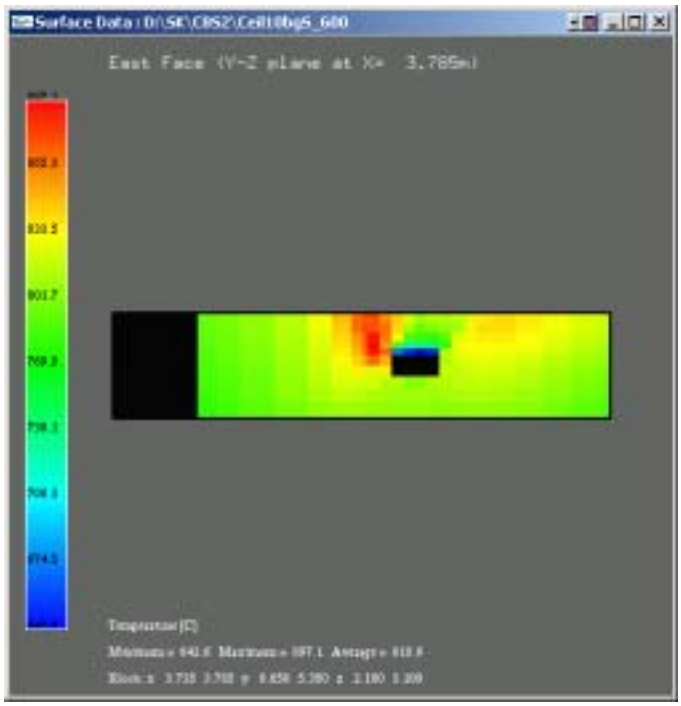


**Figure D21 Temperature contours on the exposed face of the cavity barrier**

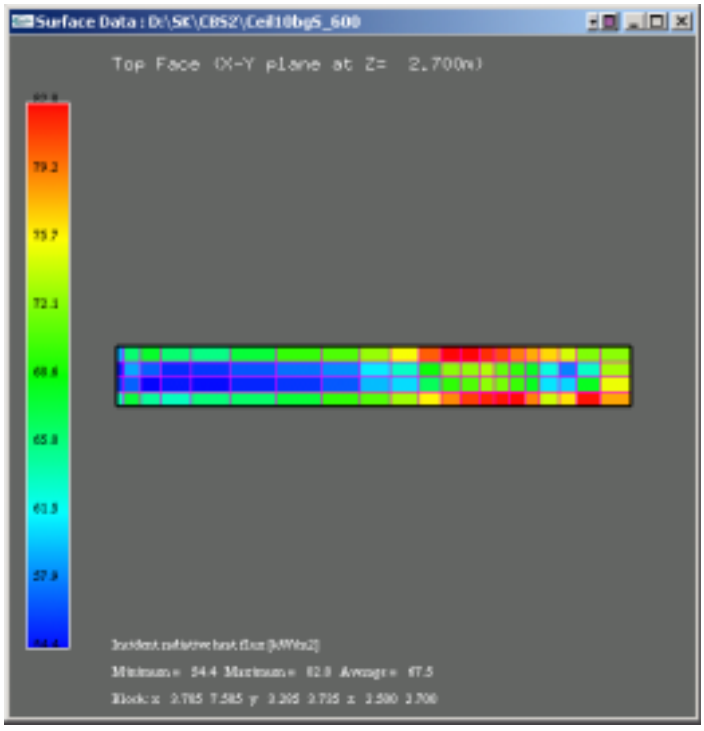


Figure D22 Temperature contours on the unexposed face of the cavity barrier

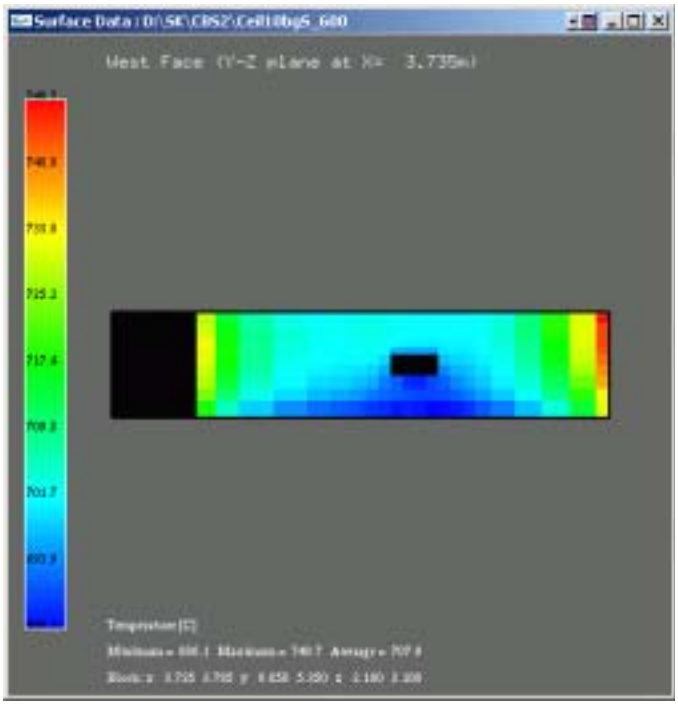


Figure D23 Incident radiative flux on the top surface of the burning cable (from the burner flames)

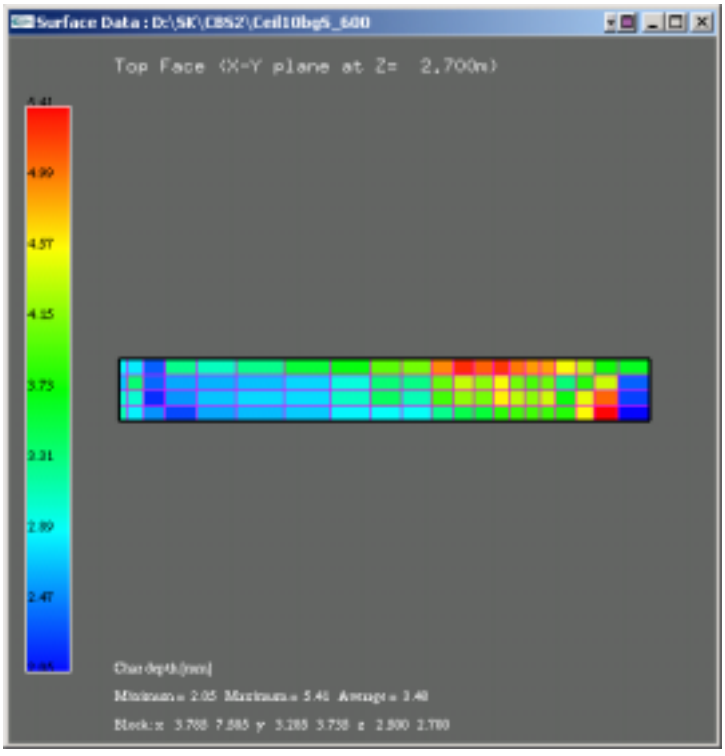


Figure D24 Char depth representing the burnt out of the cable at 5 minutes from ignition

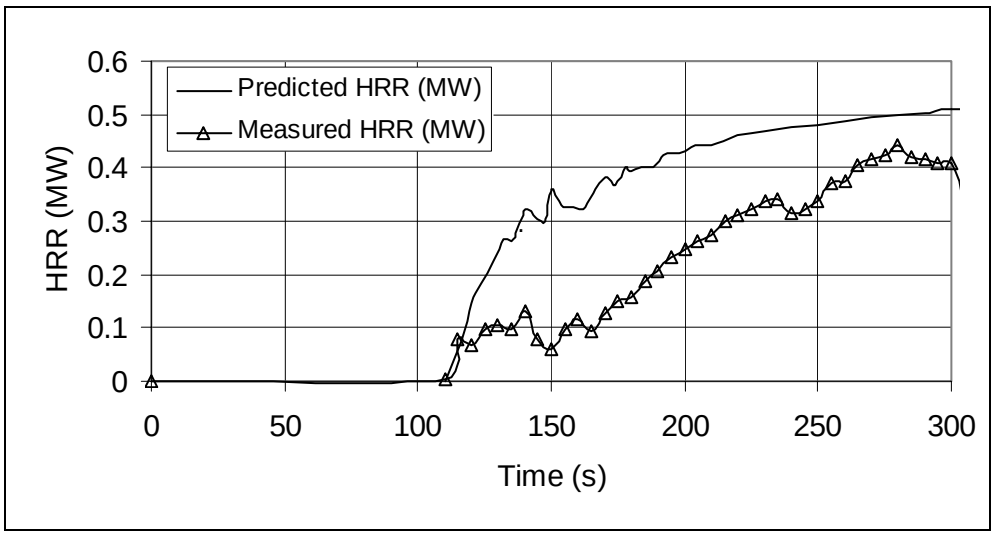


Figure D25 Predicted and measured heat release rate from the burning PVC communication cable.